

InP- and Graphene-based grating-gated transistors for tunable THz and mm-wave detection

Nima Nader Esfahani^{a,b}, Justin W. Cleary^c, Robert. E. Peale^b, Walter R. Buchwald^a, Christopher J. Fredricksen^b, Joshua Hendrickson^c, Michael S. Lodge^d, Ben D. Dawson^d, and M. Ishigami^d

^aSolid State Scientific Corporation, 12 Simon St. Nashua, NH 03060;

^bDepartment of Physics, University of Central Florida, Orlando FL, USA 32816;

^cAir Force Research Laboratory, Sensors Directorate, Wright Patterson AFB OH 45433

^dDepartment of Physics and Nanoscience Technology Center, University of Central Florida, Orlando, FL 32816

ABSTRACT

Plasmon excitation in the two dimensional electron gas (2DEG) of grating-gated high electron mobility transistors (HEMTs) gives rise to terahertz absorption lines, which may be observed via transmission spectroscopy. Such absorption resonances may alter the channel conductance, giving a means for tunable terahertz detection. The transmission spectrum may be calculated analytically by making simplifying assumptions regarding the electron distribution. Such assumptions can limit the usefulness of such analytical theories for device optimization. Indeed, significant differences between experimentally observed resonances and theory have been noted and explained qualitatively as due to additional, unanticipated, sheets of charge in the device. Here, we explore finite element method (FEM) simulations, used to obtain realistic carrier profiles. Simulated plasmon spectra do not support previous explanations of red-shifting due to interactions with additional neighboring charge distributions. Simulations do show unexpected plasmon resonances associated with the unanticipated sheet charge, named virtual-gate, as well as the expected resonances associated with the 2DEG. Plasmonic modes determined from these investigations are able to account for the measured absorption lines which were previously thought to be red-shifted 2DEG plasmons. Additionally, the same simulation approach was applied to proposed graphene-based devices to investigate their plasmon resonance spectra.

Keywords: HEMT, Plasmon, terahertz, 2DEG

1. INTRODUCTION

Grating-gated high electron mobility transistors have potential as broadly tunable terahertz detectors [1] based on resonant excitation of plasmons in the 2DEG layer by incident electromagnetic waves. The induced grating polarization generates local fields that set up standing plasma oscillations in the 2DEG at frequencies defined by the grating wavevector, sheet charge density, and the plasmon dispersion relation [2]. Changing the sheet charge density by external gate bias tunes the plasmon frequency. The excitation of plasmons results in significant absorption of the incident electromagnetic wave [3], as has been observed by transmission spectroscopy in Si [2], AlGaAs [1], GaN [4], and InP [5] materials systems. In some cases, this excitation gives rise to a resonant change in channel conductance [1], which provides the basis for possible tunable electrical detection at THz wavelengths.

Figure 1 (left) presents the layered structure of one particular InP/InGaAs HEMT structure that has been well investigated [5,6]. The different colored regions identify different materials as identified in the caption. The 2DEG is located at the interface of the 4.5 nm thick InAlAs layer and the 40 nm InGaAs channel at 44.5 nm below the grating. Charge carriers trapped by the quantum well (2DEG) are provided by the 20 nm thick Silicon-doped ($2 \times 10^{18} \text{ cm}^{-3}$) InAlAs layer in the spacer layer. Silvaco Atlas 2-D device simulator (FEM analysis software) was used to determine the free carrier concentration profile of this manufacturer specified structure. This profile is plotted as the solid curve in Fig. 1 (left). The simulated profile indicates a maximum charge density at the 2DEG of 10^{19} cm^{-3} with a maximum charge density of $5 \times 10^{16} \text{ cm}^{-3}$ remaining in the barrier.

Measured transmission spectra of the device were reported in [5]. The observed resonance frequencies were significantly red-shifted from those predicted by analytical theory. The shift was attributed [7,8] to a “virtual-gate” formed by the layer of free charge remaining in the barrier region (Fig. 1, left). However, the additional concentration of charge in the virtual gate may have its own plasmonic excitations at frequencies well below those expected for the 2DEG. Exploration of this suggestion motivates the present investigation by numerical approach, since existing analytical theory seems ill-equipped to deal with this complicated charge distributions [7].

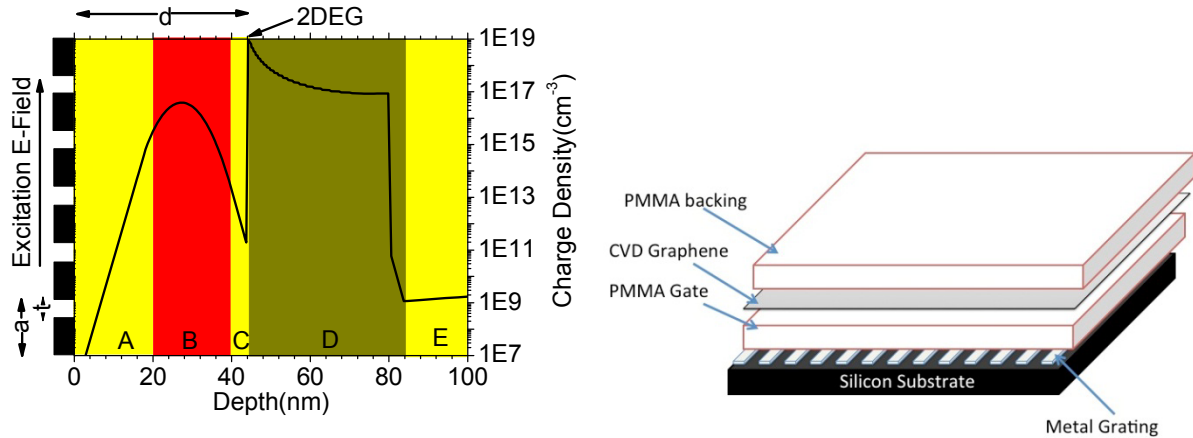


Fig. 1. (left) Structure of InP/InGaAs HEMT device along with its diagram of electron concentration, with A: Undoped In_{0.52}Al_{0.48}As, B: Si-doped In_{0.52}Al_{0.48}As, C: In_{0.52}Al_{0.48}As Setback, D: In_{0.53}Ga_{0.47}As Channel and E: undoped In_{0.52}Al_{0.48}As Buffer. (right) Schematic of a Graphene device.

Additionally, we also investigated similar plasmon resonances in a Graphene-based HEMTs (Fig. 1, right). CVD-grown Graphene with cm-scale dimensions, together with initial far-IR transmission measurements and analytical theoretical predictions for plasmon resonance lineshapes and tuning were presented in [9,10]. In contrast to conventional 2DEGs in HEMTs, for which the plasmon frequency goes as the square root of the sheet charge density n_s , it was found that the plasmon frequency of these Graphene-based devices goes as the fourth root of n_s [10,11]. Moreover, there was the predicted potential for broad tunability up to 10 THz and resonances persisting up to room temperature.

2. THEORETICAL CONSIDERATIONS

A modified Drude model for highly doped semiconductors is used to calculate the frequency-dependent permittivity and conductivity of the layers in the structure. First the plasma frequency and the relaxation time of the semiconductor are calculated using

$$\omega_p^2 = \frac{Ne^2}{m^*m_e\epsilon_\infty\epsilon_0}, \quad (1)$$

and

$$\tau = \frac{\mu m^* m_e}{e}, \quad (2)$$

where ϵ_0 is the free space permittivity, ϵ_∞ the high frequency limit of permittivity, m^* the electron effective mass, m_e the free electron mass, e the electron charge, μ the mobility, and N the carrier concentration. The frequency-dependent complex permittivity (ϵ) and conductivity (σ) are then found by

$$\epsilon(\omega) = \epsilon_\infty \left(1 - \frac{\omega_p^2 \tau}{\omega^2 \tau + i\omega} \right), \quad (3)$$

and

$$\sigma(\omega) = \frac{Ne^2\tau}{m^*m_e} \frac{1}{1 - i\omega\tau} \quad (4)$$

where ω is the frequency and all other symbols as previously defined. The permittivities used in all doped regions were complex. Real and imaginary parts are denoted by primes, e.g. $\epsilon = \epsilon' + i\epsilon''$. The conductivities used in all regions with doping were complex with the exception of the narrow regions around the peak carrier concentration in the virtual-gate and the 2DEG, where only the real parts of the conductivity were used [5].

Graphene requires special treatment since the electron effective mass is zero. In simulations of graphene-based HEMTs, the quantity m^*m_e is replaced in above relations by

$$\frac{\hbar\sqrt{\pi n_s}}{v_f} \quad (5)$$

In Eq. 5, v_f is the Fermi velocity.

The dispersion relation for plasmons inside the 2DEG of a high electron mobility transistor is given by [2]

$$\omega_p^2(x=d) = \frac{e^2 n_s q}{m^* m_e \epsilon_0 (\epsilon_s + \epsilon_d \coth(qd))} \quad (6)$$

where q is the plasmon wavevector, which can take discrete values of $2\pi n/a$, where a is the grating period and n is an integer defining harmonics of the fundamental plasmon absorption.

Silvaco Atlas 2-D FEM analysis software, has already been mentioned as our method, used to determine the free carrier concentration profile according to the manufacturer specified structure and doping. COMSOL Multiphysics (FEM software) was used to calculate electric field distributions and the transmittance spectra.

3. RESULTS

3.1 InP/InGaAs HEMT

FEM calculation of free carrier concentration profiles are presented in Fig. 1 (left). Previous investigations on the red-shift associated with the plasmon resonances for the structure with respect to predictions of analytic theory speculated increased inertia from coupling between the 2DEG and virtual-gate [7,8], and the results could be reasonably explained with a more complicated dispersion relation derived for this situation [7]. To explore this idea further, we first performed FEM calculated carrier distributions for doping levels of 2, 2.4, and 2.8 $\times 10^{18} \text{ cm}^{-3}$ are presented in Fig. 2. We found in all cases a 2DEG concentration of $1.44 \times 10^{19} \text{ cm}^{-3}$ confined to a 3 nm layer. In contrast, the peak concentration within the virtual-gate (located 15 nm above the 2DEG) was found to depend strongly on doping. For $2 \times 10^{18} \text{ cm}^{-3}$ doping, the virtual-gate peak concentration is $5 \times 10^{16} \text{ cm}^{-3}$, while for $2.8 \times 10^{18} \text{ cm}^{-3}$ doping, the virtual-gate peak is $1 \times 10^{18} \text{ cm}^{-3}$. In other words, a factor of just 1.4 increase in doping causes a factor of 20 increase in virtual-gate concentration.

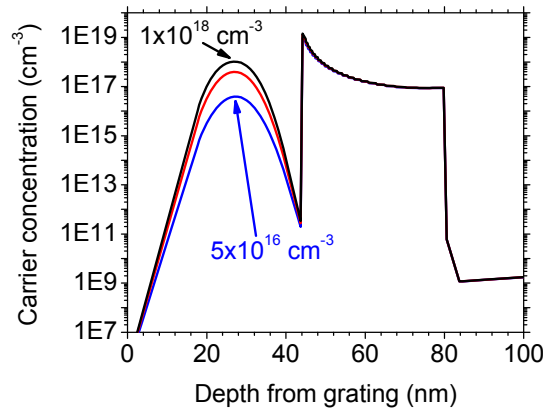


Fig. 2. Calculated electron concentration profile inside different layers of HEMT structure as a function of depth for dopant concentrations $2, 2.4, \text{ and } 2.8 \times 10^{18} \text{ cm}^{-3}$ in the InAlAs layer above the 2DEG well. Peak concentrations in the virtual-gate are found to be $5 \times 10^{16}, 4 \times 10^{17}, \text{ and } 1 \times 10^{18} \text{ cm}^{-3}$, respectively.

COMSOL Multiphysics (FEM software) calculations demonstrate the range of possible plasmon resonances excited by THz radiation. The period of the modeled infinitely long grating was $0.5 \mu\text{m}$, which is much less than the minimum $\sim 50 \mu\text{m}$ wavelength considered. The grating duty was 20%, i.e. the gaps between grating bars were 80% of the period. Five different HEMT structures were investigated, three of which were presented in Fig. 2. Two fictional profiles are also used to investigate how the 2DEG and virtual-gate act independently, with both being derived from the lowest concentration curve in Fig. 2. The first case uses only the carrier profile region of the virtual-gate (the spacer region) while the 2DEG and channel region of the device remain undoped. Oppositely, the second case leaves the spacer region (virtual-gate) completely undoped while retaining the doping profile of the 2DEG and channel region.

The three carrier profile curves in Fig. 2 determine N as a function of distance from the grating-gate. These profiles are used in COMSOL to investigate how plasmon resonances change with electron concentration in the virtual-gate. The virtual-gate is treated as a 2DEG: We picked a 3nm layer with the peak carrier concentration in doped InAlAs layer and defined it as a 2DEG by giving it real conductivity [5]. Permittivity and conductivity were found from Eqs. 1-4 with other InGaAs parameters taken to have values $\mu = 17,800 \text{ cm}^2/\text{V}\cdot\text{s}$, $\tau = 0.44 \text{ ps}$, $m^* = 0.043$, and $\epsilon_\infty = 13.65$ [5]. For the InAlAs virtual-gate region, the mobility was chosen to be the same as the InGaAs. Other values for InAlAs were $\tau = 0.81 \text{ ps}$, $m^* = 0.08$ [12] and $\epsilon_\infty = 12.24$.

Figure 3 presents COMSOL results of the transmittance spectrum of a device with a virtual-gate peak concentration of $1 \times 10^{18} \text{ cm}^{-3}$. The transmittance is calculated by integrating over the normalized electric field in the substrate region of the HEMT and then dividing by the same normalized electric field when no grating is present. The inset of the graph shows the same plot but magnified to better visualize the line labeled “B” at 99.7 cm^{-1} . The full width at the half maximum of the absorption line “B” is 0.7 cm^{-1} . Two strong lines appear above line “B”. A second weaker grouping of distinct well separated lines occurs in the range $10\text{-}60 \text{ cm}^{-1}$. The line labeled “A” occurs at 14.7 cm^{-1} .

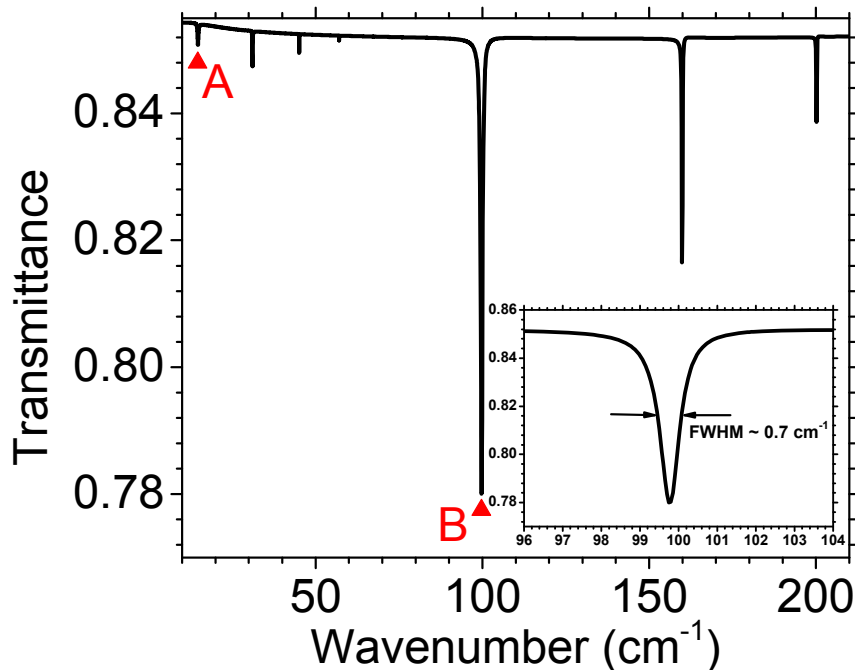


Fig. 3. Simulated plasmonic transmittance spectrum for a HEMT structure with $1 \times 10^{18} \text{ cm}^{-3}$ peak carrier concentration inside doped-InAlAs virtual-gate layer. Lines marked by arrows at frequencies, 14.7, 99.7, and labeled “A”, “B”, are associated with modes pictured in Figs. 5-6.

We first note that to support a plasmon at a particular frequency, an electron concentration must be metallic at that frequency. This is equivalent to having a real part of the permittivity that is negative. Figure 4 presents calculations of ϵ' spectra for electron concentrations of $1 \times 10^{18} \text{ cm}^{-3}$ and $1 \times 10^{19} \text{ cm}^{-3}$ for virtual-gate and 2DEG, respectively. The high concentration of the 2DEG insures that its permittivity is negative, and that it can support plasmons, over the entire range of interest. In contrast, the virtual-gate has negative permittivity only below 284 cm^{-1} . One sees that at $\sim 15 \text{ cm}^{-1}$, the permittivity of the virtual-gate has the same value as that of the 2DEG at $\sim 100 \text{ cm}^{-1}$. Therefore, from the point of view of macroscopic electrodynamics, if the 2DEG supports a plasmon at $\sim 100 \text{ cm}^{-1}$, the virtual-gate should support one at $\sim 15 \text{ cm}^{-1}$. The COMSOL simulations support the existence of both plasmon resonances, which we identify as lines “A” and “B” in Fig. 3 and which are investigated in more detail below.

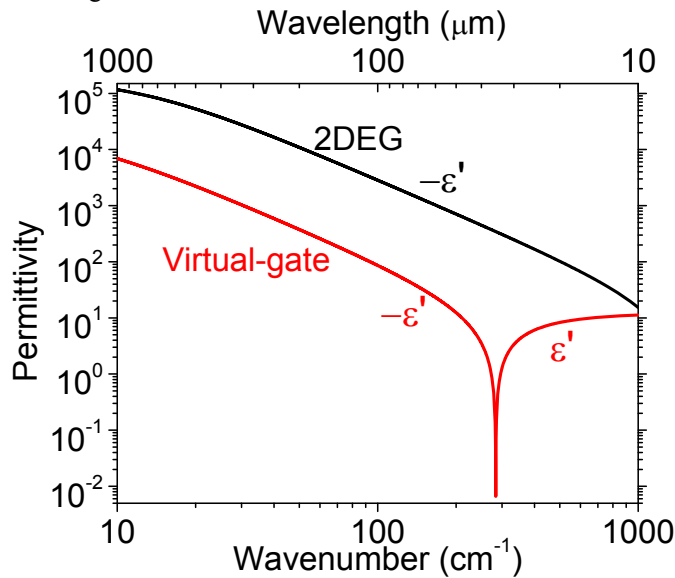


Fig. 4. Calculated permittivity of 2DEG (Black) and virtual-gate (red) for a HEMT structure with $1 \times 10^{18} \text{ cm}^{-3}$ peak carrier concentration inside doped-InAlAs layer.

Figures 5-6 present calculated THz electric-field distributions for the electron distribution used for Figs. 3 and 4. At the top of each figure are the outlines of the cross sections of two of the grating bars. The horizontal lines in figures 5-6 are subdivisions of the space to allow simple functional representations of the Silvaco-determined electron distribution (Figs. 1 and 2) within each region. The virtual-gate region is divided into 3 regions with different $N(y)$ functions, and the 2DEG into 2-3.

The color in Figures 5-6 indicates the magnitude and sign of the calculated ΔE_y in the vertical component of the electric field E_y . This change is caused by increases and decreases in the sheet charge density as compared to the average charge density, such as would be caused by (e.g.) a standing plasma wave excited by normally incident THz radiation. Intense blue color indicates a large negative value for ΔE_y , while intense red color indicates a large positive value. The most intense red or blue color corresponds to a field change of $\sim 2500 \text{ V/m}$, which implies a change in the 2D charge density of about 0.0004%. When no plasmon mode is excited, only weak fields due to the polarization of the grating by the incident THz radiation are observed [7].

Figure 5 presents the calculated ΔE_y when the first order plasmon is excited within the 2DEG, which occurs at 99.7 cm^{-1} and corresponds to the strongest peak labeled “B” in Fig. 3. Where there is a plasmon-induced increase in electron concentration in the 2DEG, the color is blue above and red below. Where there is a plasmon-induced electron concentration decrease, the ordering of the colors is reversed. The inset in Fig. 5 is a magnified view with the positions of the virtual-gate and the 2DEG labeled. There is apparently little change in the electron concentrations within the virtual-gate, since the color is continuous across this layer. These results indicate that for the wave vector defined by the grating period, incident THz radiation at 99.7 cm^{-1} excites a standing plasma wave in the 2DEG, but it does not do so in the virtual-gate.

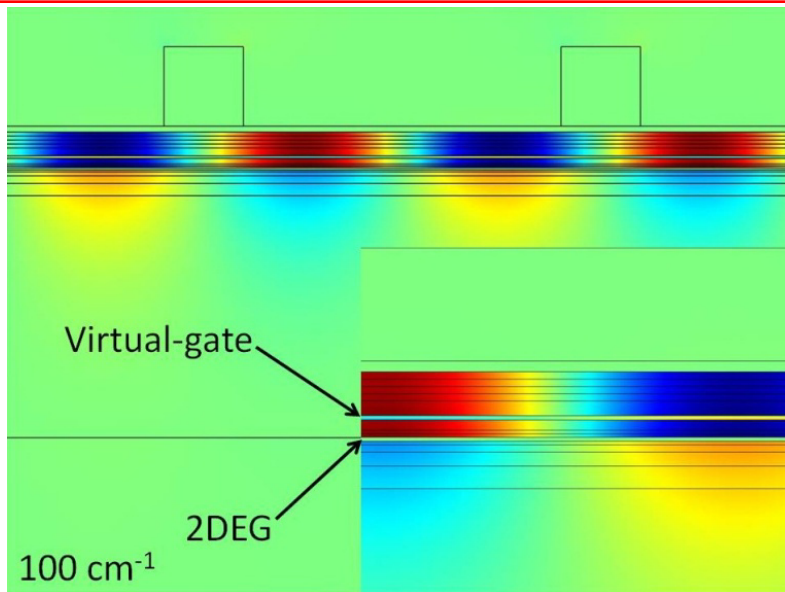


Fig. 5. Modes associated with fundamental resonant absorption at 99.7 cm^{-1} by plasmons in the 2DEG.

Fig. 6 presents a ΔE_y plot at a frequency of 14.7 cm^{-1} , which corresponds to the weak line labeled “A” in Fig. 3. The fields change sign across the virtual-gate with horizontal period equal to the grating period. Thus, these fields correspond to a fundamental plasmon resonance within the virtual-gate. The ΔE_y value is continuous across the 2DEG showing that there is no plasmon excitation within this layer. The fundamental plasmon frequency of the virtual-gate is 7.8 times lower than that of the 2DEG. This factor is larger than $\text{Sqrt}[10]$, where 10 is the ratio of the sheet charge density in the two layers, which would be the concentration dependence expected if both charge layers were at the same depth d for the simplest dispersion relation. However, that the virtual-gate is closer to the grating gate increases its coupling to the gate electrons, which increases inertia and reduces the plasma frequency [3].

The magnified inset view shows an absence of any field change within the virtual-gate itself. This may be explained by additional vertical charge polarization since the thickness of the virtual-gate is finite. This vertical polarization screens the interior of the virtual-gate from the fields. The region below the 2DEG seems to be screened by the high charge density there, making ΔE_y almost imperceptibly small.

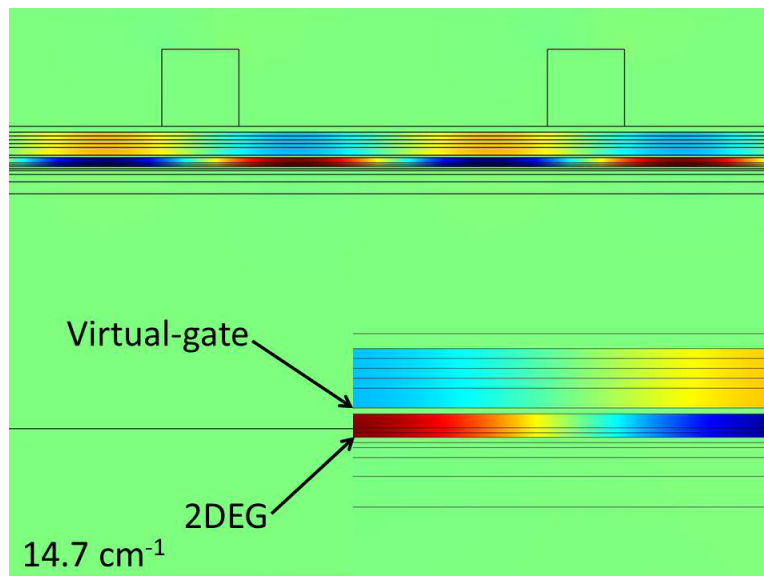


Fig. 6. Modes associated with fundamental resonant absorption at 14.7 cm^{-1} by plasmons in the Virtual-gate.

Similar calculations of transmission spectra and mode analysis have been performed for the four other doping profiles considered. Figure 7 (Left) summarizes the results. Modes associated with plasmons in the virtual-gate are marked with closed triangles, and modes associated with plasmons in the 2DEG are marked with closed circles. The resonance order of each of the modes is labeled in the figure. The three carrier profiles in Fig. 2 are labeled by their peak virtual-gate concentration on the y-axis of Fig. 7 (Left). Two fictional profiles explained earlier in the text are marked as 2DEG and virtual-gate in the figure.

Frequencies of 2DEG plasmons shift minimally with doping concentration, because the carrier concentration in the 2DEG also changes minimally (Fig. 2). In contrast, features associated with the virtual-gate undergo a strong blueshift with increasing dopant concentration. The shift goes roughly as the square root of the concentration in the virtual-gate, as expected from the simple dispersion relation for 2D plasmons [2]. Forth order plasmonic modes inside virtual-gate for the three carrier profiles in Fig. 2 are presented with red circles in figure 7 (right), with the black line representing fits to the data as a function of square root of carrier concentration and blue line representing calculation of Equ. 6 without any fitting parameters for different values of sheet charge density.

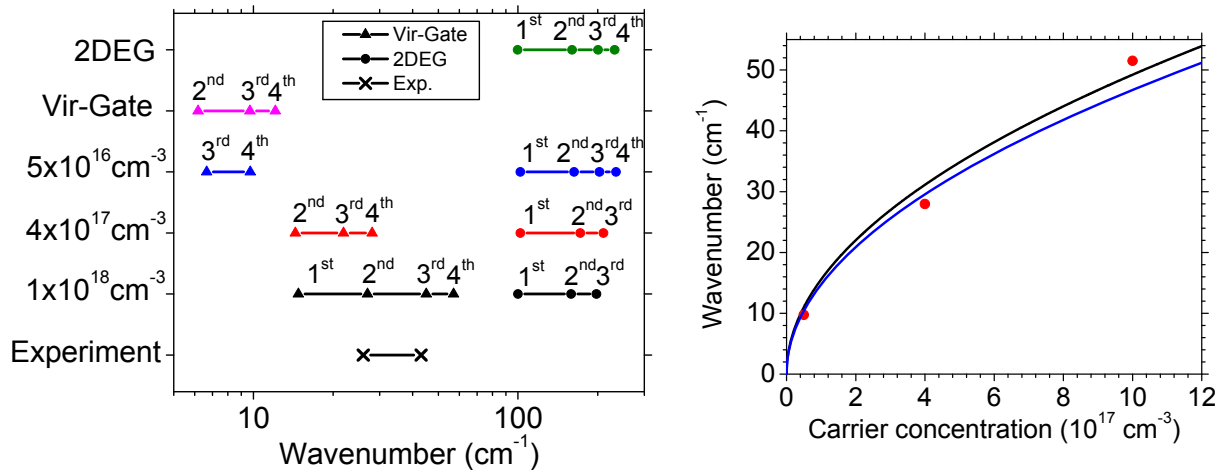


Fig. 7. (left) Results of simulations for five different profiles. Simple plasmon modes in 2DEG (solid circles) and virtual-gate (solid triangles) are numbered according to resonance order. Measured values [5] are marked with two crosses connected with a bar. **(right)** plasmon frequency vs. carrier concentration data (symbols) and fit (line).

The resonances with virtual-gate concentration $5 \times 10^{16} \text{ cm}^{-3}$ and artificially zeroed 2DEG, redshift when the 2DEG is added back in. This is caused by increased inertia duo to coupling between the two charged layers. In contrast, the resonances within the 2DEG are hardly dependent on virtual-gate concentration at all. In particular, the presence of a virtual-gate does seem unable to explain the position of the experimental data, which are strongly red-shifted compared with the calculated positions. Thus, the explanation we proposed earlier [7,8] for the discrepancy between theory and experiment is not supported by the COMSOL simulations.

Also presented in figure 7 are two experimental data points measured and reported in [5]. Empirical absorption lines match with the second and third harmonics of the plasmonic mode in the virtual-gate of the structure with the profile having the peak carrier concentration of $1 \times 10^{18} \text{ cm}^{-3}$ inside virtual-gate. Thus, we reach a suggestive alternate explanation for the resonances reported in [5], namely that they are harmonics of plasmons that occur in the virtual gate, and they are not plasmons within the 2DEG itself.

If the alternate suggestion is accepted, and considering that the virtual-gate concentration that is giving agreement corresponds to a structure with initial doping concentration of $2.8 \times 10^{18} \text{ cm}^{-3}$ (Fig. 3) while the manufacturer specified a value $2 \times 10^{18} \text{ cm}^{-3}$, we must conclude that the latter value is inaccurate by $\sim 30\%$. This was in fact speculated in [7] by means of calculating mobility of InAlAs layer using zero gate voltage conductivity and peak carrier concentration in virtual-gate.

The new interpretation of the resonances reported in [5] must still pass one additional test, namely the dependence of their frequency position on gate bias. This will require a calculation of the concentration profile under gate bias and COMSOL simulations for each such profile. Such work is now underway.

3.2 Preliminary Graphene Results

The Graphene device shown in Fig. 1 (right) is simulated utilizing COMSOL multiphysics. A schematic of the structure actually simulated is presented in Figure 8. The grating is put on top in order to make use of the same code used for the InP device, though we do not believe this should make any difference. Its period is $3.4 \mu\text{m}$ and its duty cycle (t/a) 40%. Mobility, sheet charge density, Fermi velocity and the high frequency limit of permittivity of Graphene were chosen to be $\mu = 5,000 \text{ cm/V.s}$, $n_s = 6 \times 10^{13} \text{ cm}^{-2}$, $V_f = 1 \times 10^6 \text{ m/s}$ and $\epsilon_\infty = 1$. The Graphene sheet is located 90 nm below the grating, is 5 Angstroms thick and is sandwiched between two PMMA layers. The relative permittivity of PMMA was taken to be $\epsilon = 3.3$. These values have been collected from Ref. [9].

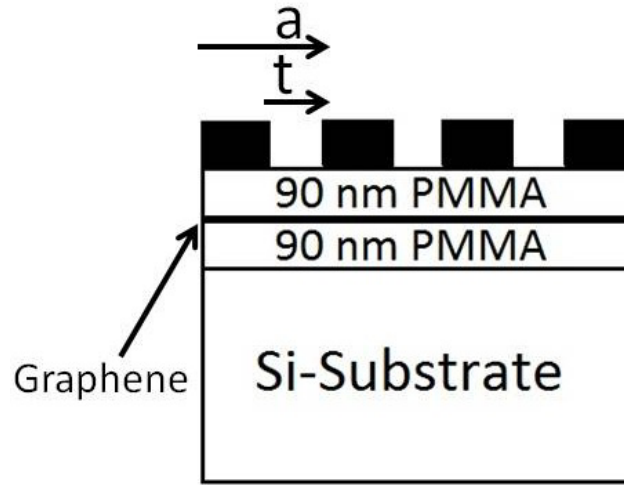


Fig. 8. Schematic of the Graphene device used in FEM simulations.

Figure 9 (left) presents COMSOL results of the transmission spectrum of the aforementioned Graphene-based device. The transmission is calculated by integrating over the normalized electric field in the substrate region of the HEMT. Four different plasmonic modes are observed as marked with red arrows. The first order plasmonic resonance occurs at a frequency of 161 cm^{-1} , with the second, third, and fourth modes occurring at 307, 435, and 544 cm^{-1} , respectively. These results are in agreement with the predictions of modified theory of two-dimensional grating couplers as investigated previously in Ref. [9].

Figure 9 (right) presents COMSOL results of ΔE_y . Shown is the first order plasmonic mode associated with the Graphene sheet which is indicated by the opposite signs of the field above and below this layer, i.e. the separation of charge in the sheet. Relatively weak electric field changes are observed in the lower PMMA.

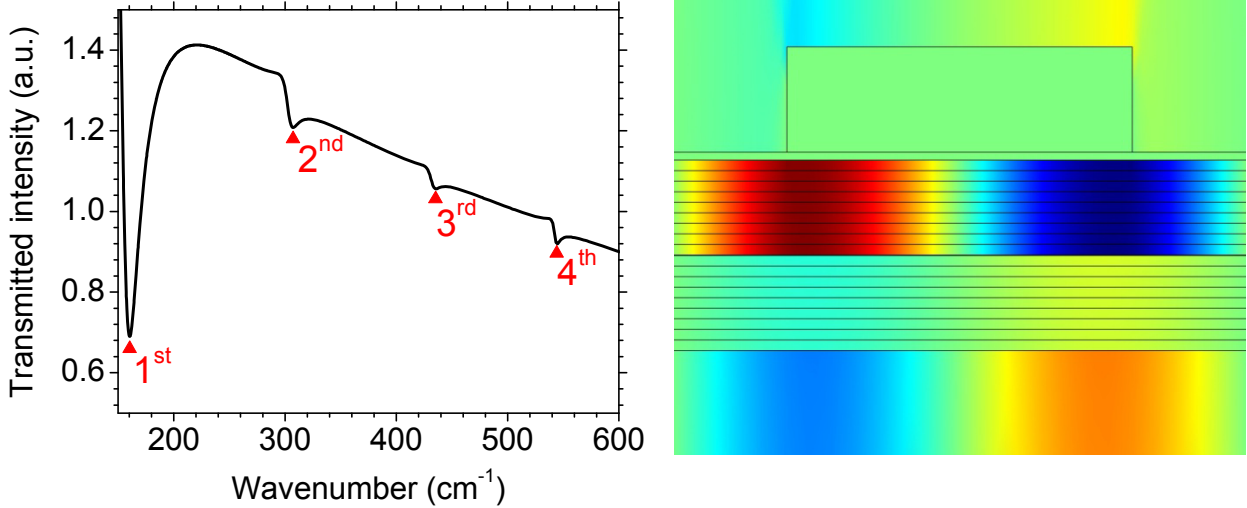


Fig. 9. Simulated plasmonic transmission spectrum for a Graphene based HEMT structure with a sheet charge density of $6 \times 10^{13} \text{ cm}^{-2}$ in the Graphene. (left) Absorption lines marked by arrows are associated with plasmonic modes and are as numbered accordingly. (right) Plot of ΔE_y in the vicinity of a grating bar for the first order plasmon mode in Graphene.

4. SUMMARY

FEM analysis utilizing Silvaco Atlas 2-D device simulator and COMSOL Multiphysics has been completed on the modeling of the InP HEMT structure presented in Fig. 1. Investigated is the effect of a virtual-gate region that is a region with high charge carrier concentration between the 2DEG and grating-gate of the structure. Two different groupings of absorption lines were identified in the transmission spectra of this device with one being from the excitation of plasmonic modes in the 2DEG. The other one is due to excitation of plasmons inside virtual-gate.

The results presented here predict a redshift for in the virtual-gate plasmons with decreasing doping density, but the effect on plasmons in the 2DEG is small. An alternate explanation for the resonant absorption lines observed in [5] is suggested, i.e. that that are due to plasmons in the virtual gate rather than in the 2DEG as previously supposed.

5. ACKNOWLEDGMENTS

NNE, JWC and JH would like to acknowledge support from the Air Force Office of Scientific Research (Program Manager Dr. Gernot Pomrenke) under contract number 12RY10COR. REP acknowledges support also by the Air Force Office of Scientific Research (Program Manager Dr. Gernot Pomrenke) under grant number FA95501010030. BDD and MI acknowledge the support by the Intelligence Community Postdoctoral Fellowship Program.

REFERENCES

- [1] Peralta, X. G., Allen, S. J., Wanke, M. C., Harff, N. E., Simmons, J. A., Lilly, M. P., Reno, J. L., Burke, P. L., and Eisenstein, J. P., "Terahertz photoconductivity and plasmon modes in double-quantum-well field-effect transistors," *Appl. Phys. Lett.*, 81, 1627-1629 (2002).
- [2] Allen, S. J., Tsui, D. C. and Logan R. A., "Observation of the Two-Dimensional Plasmon in Silicon Inversion Layers", *Phys. Rev. Lett.* **38**, 980 (1977).
- [3] Nader Esfahani, N., Peale, R. E., Cleary, J. and Buchwald W. R., "Plasmon resonance response to millimeter-waves of grating-gated InGaAs/InP HEMT," *Proc. SPIE* 8023-27 (2011)

- [4] Muravjov, A. V., Veksler, D. B., Popov, V. V., Polischuk, O. V., Pala, N., Hu, X., Gaska, R., Saxena, H., Pelae, R. E., and Shur, M. S., "Temperature dependence of plasmonic terahertz absorption in grating-gate gallium-nitride transistor structures," *Appl. Phys. Lett.* 96, 042105 (2010).
- [5] Saxena, H., Peale, R. E. and Buchwald, W. R., "Tunable two-dimensional Plasmon resonances in an InGaAs/InP HEMT", *J. Appl. Phys.* **105**, 113101 (2009).
- [6] Peale, R. E., Saxena, H., Buchwald, W. R., Dyer, G. C., and Allen, S. J., "Tunable THz Plasmon resonances in InGaAs/InP HEMT," *SPIE* 7311-17 (2009)
- [7] Cleary, J. W., Peale, R. E., Saxena, H., Buchwald, W. R., "Investigation of plasmonics in the two-dimensional electron gas of an InGaAs/InP high electron mobility transistor." *Proc. SPIE* 8023 80230X-1 (2011)
- [8] Peale, R. E., Saxena, H., Buchwald, W. R., Aizin, G., Muravjov, A. V., Veksler, B. D., Pala, N., Hu X., Gaska, R. and Shur, M. S., "Grating-gate tunable plasmon absorption in InP and GaN based HEMTs," *Proc. SPIE* 7467-25 (2009).
- [9] Nader Esfahani, N., Peale, R. E., Cleary, J., et al., "Plasmon absorption in grating-coupled InP HEMT and Graphene sheet for tunable THz detection" *Proc. SPIE* 8261-14 (2012)
- [10] Peale, R. E., Nader Esfahani, N., Fredricksen, C. J., Medhi G., Cleary, J. W., Hendrickson, J., Buchwald, W. R., Saxena, H., Edwards, O. J., Lodge, M. S., Dawson, B. D. and Ishigami, M., "InP- and Graphene-based grating-gated transistors for tunable THz and mm-wave detection", *Proc. SPIE* 8164 -7 (2011).
- [11] Ju, L., Geng, B., Horng, J., Girit, C., Martin, M., Hao, Z., Bechtel, H. A., Liang, X., Zettl, A., Shen, Y. R. and Wang F., "Graphene plasmonics for tunable terahertz metamaterials", *Nat. Nanotechnol.* 6, 630– 634 (2011)
- [12] Bhattacharyya, A., Chattopadhyay, D., and Ghosal, A., "Electron mobility of $\text{Al}_{0.48}\text{In}_{0.52}\text{As}$," *Phys. Rev. B*, 31, 2524-2525 (1985).